Time-delayed four-wave mixing using intense incoherent light

R. Beach, D. DeBeer, and S. R. Hartmann
Columbia Radiation Laboratory and Department of Physics, Columbia University, New York, New York 10027
(Received 20 May 1985)

Time-delayed four-wave mixing (TDFWM) on the $3S$-$3P$ transition in Na vapor has been studied using intense 7-nsec pulses from a broadband laser. Large-scale 1.9-psec modulation associated with the fine structure of the $3P$ state is observed throughout. At low buffer-gas pressures and low Na-vapor temperatures, pulse-induced relaxation effects are observed while at higher Na-vapor temperatures an anomalous response develops. In the normal region the TDFWM signal is interpreted in terms of either accumulated free decays or photon echoes. We estimate the relaxation induced by the excitation pulses.

INTRODUCTION

Although there have been photon-echo and four-wave-mixing studies since the early 1960s,[1,2] it is only recently through the work of Ye and Shen[3] that the intimate connection between the two has been recognized. The key to bridging the gap and exploiting this connection is to use incoherent light.

In separate experiments done by Asaka *et al.*[4] and Beach and Hartmann,[5] incoherent light has been used to generate time-delayed four-wave-mixing (TDFWM) signals. Asaka *et al.* used a broadened cw laser to generate TDFWM and was thereby able to measure relaxation on a picosecond scale. Beach and Hartmann, using pulsed incoherent light, saw structure in the picosecond regime where the excitation pulses overlapped, while still being able to generate ordinary photon echoes when there was no pulse overlap. More recent work with a pulsed excitation source has pushed relaxation measurements into the subpicosecond regime.[6] Theoretical analyses of relaxation effects have yielded significant agreement with data. Taking the view that TDFWM signals are essentially accumulated echoes, the analysis of Asaka *et al.* posits that a grating proportional to the power spectrum of the applied fields is formed and then interrogated by the selfsame fields.[4] A more general analysis has been presented by Morita and Yajima[7] which is valid for arbitrary values of T_1, T_2, and $\delta\omega$ where T_1 and T_2 are the longitudinal and transverse relaxation times and $\delta\omega$ is the $1/e$ half-width of the inhomogeneous line.

Both of these last theories are steady state in character and assume that the excitation fields are weak. The TDFWM results of Beach and Hartmann cannot be explained by either of these theories because of the large excitation intensities used: what is needed is a nonperturbative analysis. Such an analysis, valid only when the excitation pulses do not overlap, has recently been presented to explain the generation of incoherent photon echoes.[5] An extension of this analysis is presented herein to explain the TDFWM behavior. New experimental results are also presented.

THEORY

In the weak excitation regime and for the case of T_1 and T_2 both large in comparison to $\delta\omega^{-1}$, Morita and Yajima's general formulas for the TDFWM signal reduce to the simple form

$$S=\int_{-\delta\omega\tau/\sqrt{2}}^{\infty} dy \exp(-y^2) , \tag{1}$$

where τ is the delay between the excitation pulses. The TDFWM signal is observed along $2\mathbf{k}_2-\mathbf{k}_1$ where $\mathbf{k}_1$ and $\mathbf{k}_2$ are the wave vectors of the excitation pulses and positive τ corresponds to the pulse with wave vector $\mathbf{k}_1$ preceding the pulse with wave vector $\mathbf{k}_2$. The above formula is plotted in Fig. 1 and should be compared with Fig. 2(a), a recent result from our laboratory. Our experimental result was obtained in a Na cell at 445 K where the shortest relevant relaxation time is the 16-nsec fluorescence lifetime of the $3P$ state. The inhomogeneous width of the Na D line on which we work is of the order of $\delta\omega=6.4\times10^9$ rad/sec, so that our result is obtained under the condition that T_1 and T_2 are large in comparison to $\delta\omega^{-1}$. Our excitation pulses were such that each Na atom experiences a pulse of effective area on the order of π so that except as regards the intensity of the excitation pulses the data shown in Fig. 2 correspond to the conditions under which the response shown in Fig. 1 was calculated. The most striking effect of the high-intensity excitation is thus seen to be the degradation of the TDFWM signal for large values of τ. Before we explain how this comes about we give a qualitative explanation of the weak-excitation result shown in Fig. 1.

Excitation pulses made from broadband laser light can be regarded as a train of incoherently phased noise spikes. We consider the case in which the output of a single such laser is divided, delayed, and recombined to provide one pulse with wave vector $\mathbf{k}_1$ and a second pulse delayed by τ and in a slightly different direction with wave vector $\mathbf{k}_2$. Thus we have two trains of correlated noise spikes. Although the phase of each noise spike is random, each correlated noise-spike pair having wave vector $\mathbf{k}_1$ and $\mathbf{k}_2$ has the same relative phase and therefore contributes

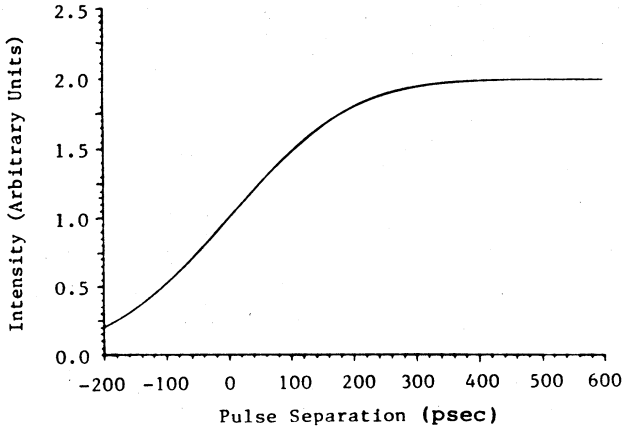

FIG. 1. Signal intensity vs excitation pulse separation after Morita and Yajima (Ref. 7) for the case in which T_1 and T_2 are both large in comparison to $\delta\omega^{-1}$.

coherently to a $\mathbf{k}_1-\mathbf{k}_2$ momentum component of the ground-state amplitude. We illustrate this in Fig. 3 by drawing only that part of the recoil diagram which shows the elements leading to this ground-state momentum buildup.[8,9] Each spike with wave vector $\mathbf{k}_1$ generates an excited-state component with momentum $\mathbf{k}_1$ which recoils as indicated by the dashed line. After a time τ the correlated noise spike with wave vector $\mathbf{k}_2$ appears and regenerates the ground state except that its momentum $\mathbf{k}_1-\mathbf{k}_2$ is not exactly zero since $\mathbf{k}_2\neq\mathbf{k}_1$. For $\mathbf{k}_2\approx\mathbf{k}_1$ the resulting ground-state trajectory for the $\mathbf{k}_1-\mathbf{k}_2$ state is effectively parallel to the original ground state with $\mathbf{k}=\mathbf{0}$. The macroscopic ground-state component with $\mathbf{k}=\mathbf{k}_1-\mathbf{k}_2$ thus develops.

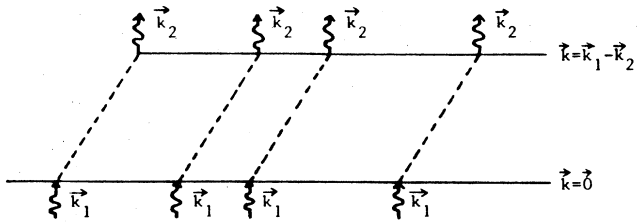

FIG. 3. Recoil diagram showing those vertices that contribute to the $\mathbf{k}_1-\mathbf{k}_2$ momentum component of the ground-state amplitude. Ground- and excited-state trajectories are denoted by solid and dashed lines, respectively.

Given a system in a macroscopic superposition of two ground states as described above it is a simple matter to find how it will radiate after subsequent irradiation. Consider, as in Fig. 4, excitation by a noise spike with wave vector $\mathbf{k}_2$ of the ground-state amplitude component with $\mathbf{k}=\mathbf{0}$. This state recoils with momentum $\mathbf{k}_2$ and crosses the ground-state component with $\mathbf{k}=\mathbf{k}_1-\mathbf{k}_2$ a time τ later. This is the classical echo formation process. The echo so produced has momentum $\mathbf{k}_2-(\mathbf{k}_1-\mathbf{k}_2)=2\mathbf{k}_2-\mathbf{k}_1$. Each noise spike with $\mathbf{k}=\mathbf{k}_2$ produces such an echo (in addition to aiding in the macroscopic ground-state formation shown in Fig. 3). These echoes add incoherently to provide the TDFWM signal. While we have called the radiated signals "echoes," this identification is not so clear when τ becomes smaller than the inverse inhomogeneous width. Echoes generally appear as a rephasing of a dephased system and radiate throughout the rephasing and dephasing process. But when τ is too small, the initial dephasing is incomplete and consequently the interval during which appreciable radiation takes place is reduced, with a corresponding reduction in signal intensity. For $\tau=0$ there is no initial dephasing and half the potential

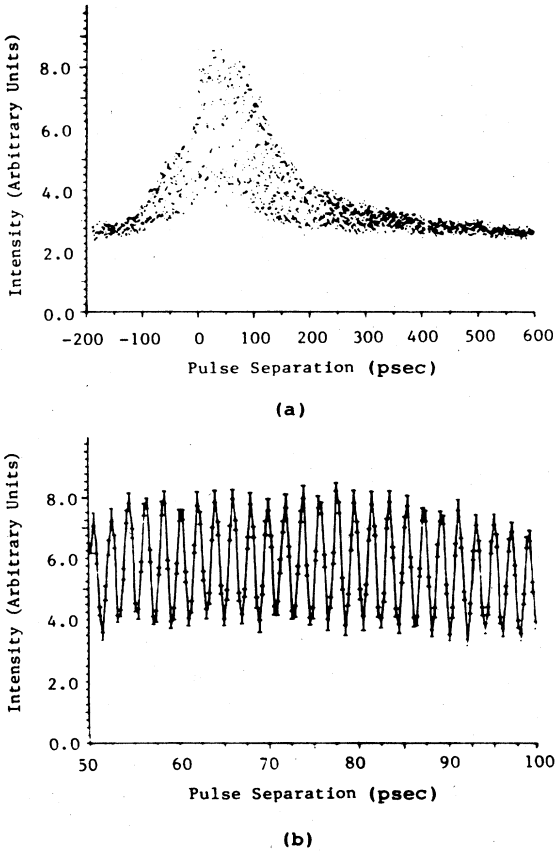

FIG. 2. (a) Experimentally measured signal intensity vs excitation pulse separation in a 10-cm-long Na cell at 445 K. (b) The same data for pulse separations of 50–100 psec with error bars and lines connecting the data. The 1.9-psec modulation is due to the Na $3P$ fine-structure beating.

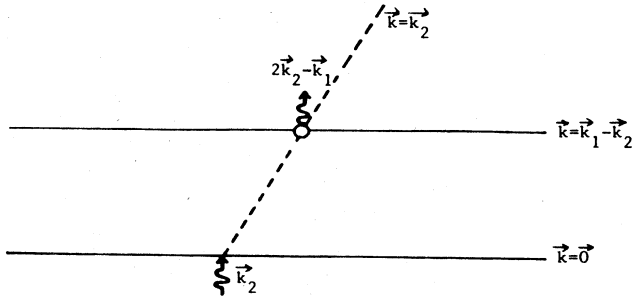

FIG. 4. Recoil diagram showing the lowest-order contribution to the signal emitted in the $2\mathbf{k}_2-\mathbf{k}_1$ direction.

echo signal is lost. For τ negative the macroscopically produced ground-state component has wave vector $\mathbf{k}=\mathbf{k}_2-\mathbf{k}_1$. A noise spike with wave vector $\mathbf{k}_2$ generates from this state an excited state with wave vector $2\mathbf{k}_2-\mathbf{k}_1$ as indicated in Fig. 5. This state and the ground-state component with $\mathbf{k}=0$ again combine to radiate along $2\mathbf{k}_2-\mathbf{k}_1$. This signal is large only for τ small; for nonzero τ it is a normal free decay less that part which would have been radiated between $t=0$ and τ. In terms of the diagrams we would say this situation corresponds to having a virtual crossing a time τ before the noise spike appears.

The discussion of the recoil diagrams can be summarized by observing that superposition states with relative wave vector $2\mathbf{k}_2-\mathbf{k}_1$ always radiate but do so with an intensity proportional to $\exp(-\Delta t^2\delta\omega^2/2)$ where Δt is the time to the (real or virtual) crossing. In the "billiard-ball" model this exponential factor gives the overlap between the superposition states.[9] In classical analysis the exponential factor represents Doppler dephasing. In any event each noise spike with wave vector $\mathbf{k}_2$ generates a signal along $2\mathbf{k}_2-\mathbf{k}_1$ proportional to $\exp[-(t-\tau)^2\delta\omega^2/2]$ where t is the interval between the arrival time of the spike with wave vector $\mathbf{k}_2$ and the time at which the signal is observed. Integrating over all t yields

$$S=\int_0^\infty dt\exp[-(t-\tau)^2 d\omega^2/2] \tag{2}$$

which is identical to the result of Morita and Yajima in Eq. (1). Our picture thus shows that TDFWM signals for positive τ are best thought of as accumulated echoes while for negative τ they arise from accumulated free decays.

In order to go beyond the low-intensity limit we need to consider those diagrams which give rise to the ground-state amplitudes suggested in Fig. 6. With this more-involved grating structure a second kind of contribution to the TDFWM signal along $2\mathbf{k}_2-\mathbf{k}_1$ appears, as shown in Fig. 7. Now noise spikes along $\mathbf{k}_1$ produce echoes along $2\mathbf{k}_2-\mathbf{k}_1$. These echoes are in a different class from those depicted in Fig. 4 inasmuch as they peak at 2τ, instead of τ, after the excitation noise spike. For τ negative we obtain the analog to Fig. 5 which is depicted in Fig. 8.

This differs from the situation depicted in Fig. 5 in that the virtual crossing appears 2τ, instead of τ, before the excitation noise spike. The appearance of terms with crossings 2τ away from the associated noise spikes modifies the relaxation behavior since the sensitivity to relaxation is

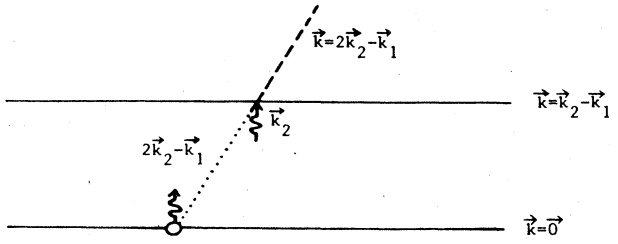

FIG. 5. Recoil diagram for the case in which τ is negative, i.e., pulse 2 precedes pulse 1 by τ. Extending the excited-state amplitude generated by the $\mathbf{k}_2$ noise spike backwards in time leads to a virtual crossing a time τ earlier giving rise to signal emission in the $2\mathbf{k}_2-\mathbf{k}_1$ direction.

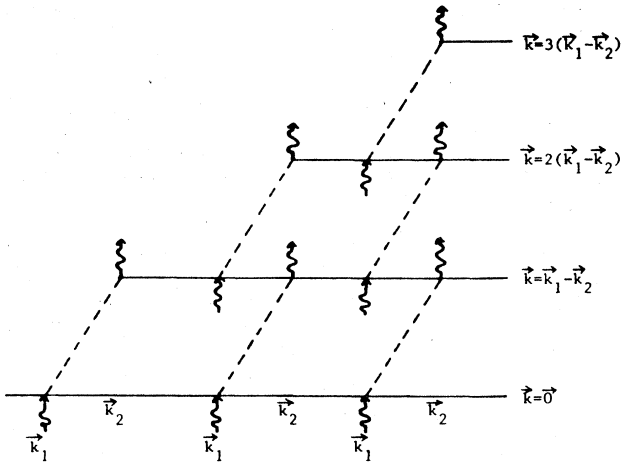

FIG. 6. Recoil diagram showing several of the various momentum components of the ground-state amplitude that are generated by intense excitation pulses.

changed. It should also be noted that as the excitation level increases, the number of terms in each of the classes presented in Figs. 4, 5, 7, and 8 increases.

Our model up to now consists of two parts. First, correlated noise-spike pairs act in unison to set up accumulated gratings and then, these gratings are interrogated by the selfsame fields to generate the TDFWM signal along $2\mathbf{k}_2-\mathbf{k}_1$. With high-intensity excitation we must also consider how the excitations affect the generated superposition states themselves, degrading the grating and radiated signal both directly and indirectly. For the purpose of this paper we consider only those signal degradation effects which depend on τ. These involve grating formation and grating interrogation and we believe they are comparable. In what follows we neglect the former but calculate the latter directly. This calculation leads to a noise-spike-induced relaxation time and is the reason for the qualitative difference between our result of Fig. 2 and the theoretical curve in Fig. 1.

For large τ, noise-spike signal degradation dominates and the TDFWM signal should diminish as we observe. As we have noted, it is important to take into account

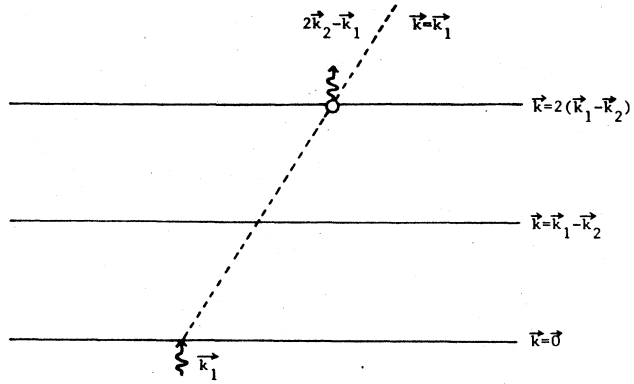

FIG. 7. A new class of recoil diagram that can contribute to the $2\mathbf{k}_2-\mathbf{k}_1$ emitted signal when the ground-state grating structure depicted in Fig. 6 is present.

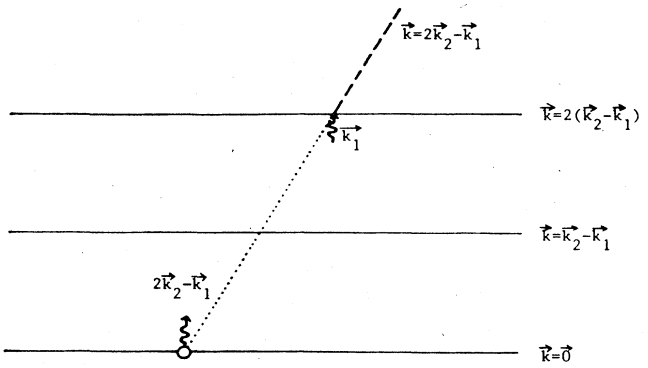

FIG. 8. Recoil diagram analogous to that depicted in Fig. 5 for the case of negative pulse separation and higher-intensity pulses. Extending the excited state generated by the $\mathbf{k}_1$ noise spike backwards in time leads to a virtual crossing a time 2τ earlier, giving rise to signal emission in the $2\mathbf{k}_2-\mathbf{k}_1$ direction.

higher-order effects when calculating the pulse-induced grating. This we do by performing a modal analysis which treats the interaction of each atomic group with its resonant mode exactly. All classes of echoes appear in the analysis which follows, and agreement with experiment is obtained within the limits of our experimental accuracy.

We must first calculate the signal along $2\mathbf{k}_2-\mathbf{k}_1$ induced by two identical but delayed broadband laser pulses along $\mathbf{k}_1$ and $\mathbf{k}_2$. We exploit the fact that the TDFWM signal comes from noise-spike scattering off the laser-pulse-induced grating. Firstly we calculate this grating, secondly we calculate the noise-spike-induced radiation from atoms in this grating, and finally we calculate the noise-spike-induced relaxation of the radiating atoms.

GRATING GENERATION

A wideband, $\Delta\Omega=2\pi t_c^{-1}$, excitation pulse of length t with correlation time t_c, if weak, interacts with those atoms which are resonant with it. More precisely, any atom whose resonant frequency, corrected for Doppler shift, is ω, interacts predominantly with Fourier components within a bandwidth $\Delta\omega=2\pi t^{-1}$ centered on ω. The interaction between an atom and Fourier components outside this bandwidth tends to average out and we therefore neglect these contributions to the laser-induced atomic grating. In this model each atom behaves, to a first approximation, as if it interacted only with a coherent narrow band light pulse. We model this pulse as having a rectangular envelope and we calculate its effect exactly.

The pulse we have described should be labeled as "effective." It is turned on at $t=0$ and has a constant amplitude. This amplitude depends on when the induced grating is to be interrogated and can be obtained from simple energy considerations. For E_t, the amplitude of the effective field used to calculate the grating at time t, the energy in a pulse of cross-sectional area A is

$$\mathscr{E}_t=\frac{c}{8\pi}E_t^2At\ . \tag{3}$$

This effective pulse energy $\mathscr{E}_t$ is related to the total energy $\mathscr{E}$ contained in the wideband laser pulse of length τ_p by the relation

$$\mathscr{E}_t=\left[\frac{1/t}{1/t_c}\right]\left[\frac{t}{\tau_p}\right]\mathscr{E}\ , \tag{4}$$

where (t/τ_p) is the fraction of $\mathscr{E}$ contained in the time interval t, and $(1/t)(1/t_c)$ is the fractional bandwidth $\Delta\omega/\Delta\Omega$ of the effective pulse. Thus

$$\mathscr{E}_t=(t_c/\tau_p)\mathscr{E} \tag{5}$$

and the effective pulse energy is independent of t. It follows then that

$$E_t^2t=E_s^2t_c\ , \tag{6}$$

where E_s is the amplitude of the noise spikes whose duration is t_c. We can therefore write the effective field $E_t(t')$ used to calculate the grating at time t as

$$E_t(t')=E_s\sqrt{t_c/t}\,\{\cos(\omega t'-\mathbf{k}_1\cdot\mathbf{r}-\varphi_t)+\cos[\omega(t'-\tau)-\mathbf{k}_2\cdot\mathbf{r}-\varphi_t]\}\ , \tag{7}$$

where $0<t'<t$.

The effect of the effective pulse on a single atom whose natural transition frequency is ω is obtained by solving

$$\frac{i}{\hbar}\frac{\partial|\psi\rangle}{\partial t'}=(H_0+PE_t)|\psi\rangle \tag{8}$$

subject to the condition that the atom is initially in the ground state, $|\psi(0)\rangle=\binom{1}{0}$. H_0 is the atomic Hamiltonian and PE_t represents the interaction with the radiation field. Since E_t is a constant-amplitude resonant pulse we can write the solution simply as

$$|\psi(t)\rangle=\begin{bmatrix}\cos(\theta_t/2)\\ ie^{i\mathbf{k}_{av}\cdot\mathbf{r}}e^{-i\omega(t-\tau/2)}e^{i\varphi_t}\sin(\theta_t/2)\end{bmatrix}\ , \tag{9}$$

where $\theta_t=2\theta_s\sqrt{t/t_c}\cos[(\Delta\mathbf{k}\cdot\mathbf{r}+\omega\tau)/2]$; where $\theta_s=PE_st_c$ is the area of a noise spike, $\mathbf{k}_{av}=(\mathbf{k}_1+\mathbf{k}_2)/2$, and $\Delta\mathbf{k}=\mathbf{k}_2-\mathbf{k}_1$. This represents the pulse-induced grating. In terms of the generating function for the Bessel function

$$\exp[i(z\cos\alpha)]=\sum_{m=-\infty}^{\infty}i^ne^{in\alpha}J_n(z)\ , \tag{10}$$

the ground-state amplitude $\cos(\theta_t/2)$ becomes

$$\cos(\theta_t/2)=\sum_{n=-\infty}^{\infty}(-1)^ne^{in(\Delta\mathbf{k}\cdot\mathbf{r}+\omega\tau)}J_{2n}(\theta_s\sqrt{t/t_c}) \tag{11}$$

which contains the hierarchy of levels shown in Fig. 6.

NOISE-SPIKE INTERROGATION

The noise-spike-induced signal is readily calculated since each noise spike can be represented by a delta function with area θ_s. Writing the wave function just calculated above as

$$\psi_-(t)=\begin{bmatrix}\psi_1\\ \psi_2\end{bmatrix}\ , \tag{12}$$

immediately after the passage of a noise spike with momentum vector $\mathbf{k}_j$ (where j is either 1 or 2) this wave

function becomes

$$\psi_+(t)=\begin{bmatrix}\psi_1\cos(\theta_s/2)+i\psi_2 e^{-i\mathbf{k}_j\cdot\mathbf{r}}e^{-i\varphi_s}\sin(\theta_s/2)\\ \psi_2\cos(\theta_s/2)+i\psi_1 e^{i\mathbf{k}_j\cdot\mathbf{r}}e^{i\varphi_s}\sin(\theta_s/2)\end{bmatrix}. \tag{13}$$

These states then freely develop as

$$\psi(t,\Delta t)=\begin{bmatrix}1 & 0\\ 0 & e^{-i\omega\Delta t}\end{bmatrix}\psi_+(t) \tag{14}$$

yielding the radiating superposition states at time Δt after excitation by a noise spike. The associated noise-spike-induced moment is

$$\langle P_s(t,\Delta t,\omega)\rangle=\langle\psi(t,\Delta t)\,|\,P\,|\,\psi(t,\Delta t)\rangle$$
$$=\frac{iP\theta_s}{2}(\psi_1\psi_1^*-\psi_2\psi_2^*)e^{-i(\omega\Delta t-\mathbf{k}_j\cdot\mathbf{r}-\varphi_s)}$$
$$+\text{c.c.} \tag{15}$$

Although we work with intense fields we have imposed the minor restriction that $\theta_s\ll 1$ in Eq. (15) for $\langle P_s(t,\Delta t,\omega)\rangle$. On writing out ψ_1 and ψ_2 this expression becomes

$$\langle P_s(t,\Delta t,\omega)\rangle=P\theta_s\cos\theta_t\sin(\omega\Delta t-\mathbf{k}_j\cdot\mathbf{r}-\varphi_s)\,. \tag{16}$$

We note that this expression is independent of the phase of the effective resonant pulse which generated the grating. But this phase is the only feature that distinguishes the various effective pulses at different frequencies which generated the associated gratings at one particular time. We can therefore combine the effects of a single interrogation noise spike on all atoms throughout the Doppler line by integrating the base formula over the linewidth. Thus

$$\langle P_s(t,\Delta t)\rangle=\int d\omega\, g(\omega)\langle P_s(t,\Delta t,\omega)\rangle\,, \tag{17}$$

where

$$g(\omega)=\frac{1}{\sqrt{\pi}\delta\omega}\exp[-(\omega-\omega_0)^2/\delta\omega^2]\,. \tag{18}$$

On combining Eqs. (16)–(18) and retaining only those terms phased to radiate along $2\mathbf{k}_2-\mathbf{k}_1$, we obtain either

$$\langle P_s(t,\Delta t)\rangle_2=P\theta_s J_2(2\theta_s\sqrt{t/t_c})e^{-\delta\omega^2(\Delta t-\tau)^2/4}$$
$$\times\sin[\omega_0(\Delta t-\tau)-(2\mathbf{k}_2-\mathbf{k}_1)\cdot\mathbf{r}-\varphi_s] \tag{19}$$

or

$$\langle P_s(t,\Delta t)\rangle_1=P\theta_s J_4(2\theta_s\sqrt{t/t_c})e^{-\delta\omega^2(\Delta t-2\tau)^2/4}$$
$$\times\sin[\omega_0(\Delta t-2\tau)-(2\mathbf{k}_2-\mathbf{k}_1)\cdot\mathbf{r}-\varphi_s]\,, \tag{20}$$

where the subscript refers to whether the interrogating noise spike had wave vector $\mathbf{k}_1$ or $\mathbf{k}_2$. For $\tau>0$ these terms correspond to the echolike diagrams shown in Figs. 4 and 7, respectively, while for $\tau<0$ they correspond to the (incomplete) free-decay-like diagrams shown in Figs. 5 and 8.

NOISE-SPIKE SIGNAL DEGRADATION

We have launched a radiating superposition state in the regime where θ_s is small but not so small that the combined action of successive noise spikes cannot have an appreciable effect on the magnitude of this superposition state. We take this into account by noting that each successive noise spike reduces the amplitude of each of the superposition states by $\cos(\theta_s/2)$ with a corresponding reduction in the induced dipole moment of $\cos^2(\theta_s/2)$. Noise spikes from each of the two excitation pulses arrive t_c apart so that the net result on the average is one noise spike every $t_c/2$ seconds. Thus in the interval Δt the induced moment is reduced by the factor $[\cos^2(\theta_s/2)]^{2\Delta t/t_c}$ and we use the fact that $\theta_s\ll 1$ to replace $\cos(\theta_s/2)$ with $\exp(-\theta_s^2/8)$ to obtain the noise-spike degradation factor for the radiated intensity

$$\eta=\exp(-\Delta t/T_s)\,, \tag{21}$$

where $T_s=t_c/\theta_s^2$.

RADIATED INTENSITY

The noise spikes which interrogate the grating are randomly phased so that the signals they produce combine incoherently. Writing $\langle P^2(t)\rangle$ as the net induced moment squared at time t the integrated intensity is

$$I=\mathscr{I}\int_0^\infty\langle P^2(t)\rangle dt \tag{22}$$

for some constant $\mathscr{I}$, where

$$\langle P^2(t)\rangle=\int_0^t dt'\langle P_s(t',t-t')\rangle h(t'-\tau_p)\,, \tag{23}$$

where $h(u)=1$ if $u<0$ and zero otherwise. We have made the dependence of P_s on t and t' explicit by using $\Delta t=t-t'$. The function $h(u)$ is introduced so that we still obtain $\langle P^2(t)\rangle$ after the noise spikes terminate at $t=\tau_p$. By changing the order of integration and replacing the integration variable t with Δt we obtain the result

$$I=\mathscr{I}\int_0^\infty dt'\int_0^\infty d(\Delta t)\langle P_s^2(t',\Delta t)\rangle h(t'-\tau_p) \tag{24}$$

which is simpler because $\langle P_s(t',\Delta t\rangle$ separates into factors depending on t' and Δt, respectively. Performing the indicated operations and combining the factor η with the induced moments we obtain

$$I=\mathscr{I}P^2\theta_s^2\left[\int_0^{\tau_p}dt\,J_2^2(2\theta_s\sqrt{t/t_c})\right]$$
$$\times\left[\int_0^\infty d(\Delta t)e^{-\delta\omega^2(\Delta t-\tau)^2/2-\Delta t/T_s}\right]$$
$$+\mathscr{I}P^2\theta_s\left[\int_0^\infty dt\,J_4^2(2\theta_s\sqrt{t'/t_c})\right]$$
$$\times\left[\int_0^\infty d(\Delta t)e^{-\delta\omega^2(\Delta t-2\tau^2)/2-\Delta t/T_s}\right]. \tag{25}$$

We note that for $\theta_s\sqrt{\tau_p/t_c}\ll 1$ and $\delta\omega\gg T_s^{-1}$ only the term involving J_2 contributes so finally,

$$I\sim\int_0^\infty d(\Delta t)\exp[-\delta\omega^2(\Delta t-\tau)^2/2]\,, \tag{26}$$

which is identical to Eqs. (1) and (2) as obtained by Morita and Yajima.

EXPERIMENTAL

Our experimental apparatus generated 7-nsec-long incoherent excitation pulses from a dye solution consisting by volume of 50% R610 ($10^{-3}M$ in CH_3OH) and 50% Kiton Red ($3\times10^{-4}M$ in CH_3OH) in a stirred dye cell, pumped by the second harmonic of a Quanta Ray DCR-1A yttrium-aluminum-garnet (YAG) laser. The dye cell was placed in an open-ended cavity with a diffraction grating in the Littrow configuration at the closed end to provide bandwidth narrowing. The output was amplified twice in two longitudinally pumped flowing dye cells containing a solution of R590 ($5\times10^{-5}M$ in CH_3OH) as shown in Fig. 9. A spectroscopic analysis of these output pulses showed them to have a central wavelength of 5893 Å and a full width at half maximum (FWHM) of between 6 and 12 Å depending on the grating used in the closed end of the cavity. Using the apparatus shown in Fig. 10 each output pulse was split in two and recombined to provide two well-defined almost parallel light pulses. We generally made the angle between the light pulses of the order of a few milliradians. The mirror $M1$ in Fig. 10 was on a translational mount driven by a computer-controlled stepper motor so that a variable delay could be inserted between the two pulses. Beyond a 10-cm-long sample cell containing Na vapor, a signal was detected in the $2\mathbf{k}_2-\mathbf{k}_1$ phase-matching direction using a spatial filtering technique. The signal intensity was detected by an EG&G FND 100 photodiode and after being integrated over the pulse duration was stored by a computer. A typical data run consisted of measuring integrated signal intensity as a function of delay as mirror $M1$ was moved through a range corresponding to ~1 nsec in delay time. Care was taken to insure that both the immediate and delayed components of the excitation beam saw the same dispersive optical elements after being split off from the single incoming pulse.

The data shown in Fig. 2 were obtained in a 10-cm cell at 445 K where the Na vapor density was $3\times10^{12}/cm^3$. At line center the sample is optically thick so the theory we have presented is strictly valid only in the wings of the resonance line. Nevertheless it is still instructive to apply the theory to this case.

Before proceeding we note that the oscillatory behavior revealed on the expanded segment shown in Fig. 2(b) is due to the coherent beating of the sodium D lines at 5889.95 and 5895.92 Å. Our laser bandwidth of 12 Å completely covers these lines which are separated by 6 Å. The beating has a period of 1.9 psec which corresponds to this wavelength separation.

For the broadband laser pulse considered as a train of incoherent noise spikes, these spikes have a nominal duration determined by the relation $\Delta\omega t_c=2\pi$ where $\Delta\omega=2\pi c\Delta\lambda/\lambda^2$ is the bandwidth $\Delta\omega$ corresponding to $\Delta\lambda$. For $\Delta\lambda=12$ Å we find the noise-spike duration is $t_c=1$ psec. The laser pulses were 7 nsec long and had an

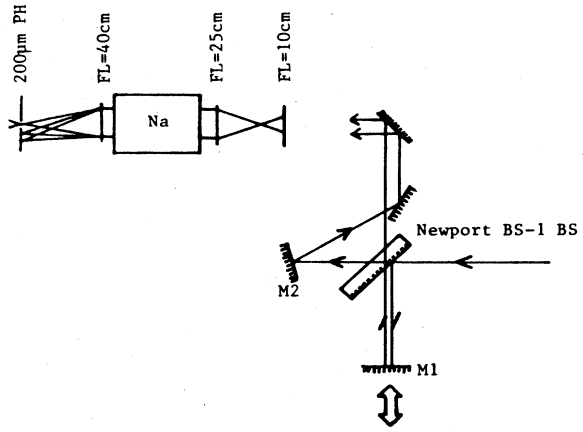

FIG. 10. Apparatus used to split apart and recombine the excitations. Mirror $M2$ is fixed while mirror $M1$ is moveable in the direction of the arrow so that a variable delay can be inserted in the beams. All mirrors in the diagram are front surface aluminum. BS stands for beam-splitter. FL stands for focal length and all such indicated lenses are achromats. The 200-μm PH was placed in the focal plane of the 40-cm lens and positioned to pass the signal emitted in the $2\mathbf{k}_2-\mathbf{k}_1$ direction while blocking the signal in the $\mathbf{k}_1$ and $\mathbf{k}_2$ directions.

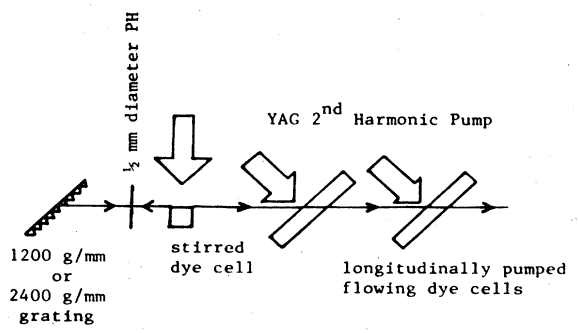

FIG. 9. Schematic diagram of apparatus used to generate the incoherent excitation pulses used in our experiment. The large arrows denote the YAG second-harmonic pump beams and PH stands for pinhole.

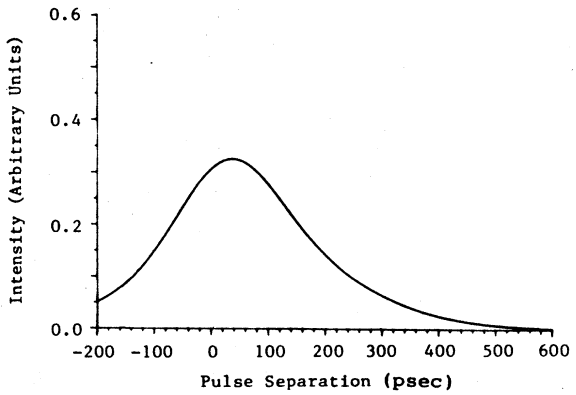

FIG. 11. A plot of our theoretical intensity vs pulse separation as given in Eq. (25) using the same parameters that describe the experimental data plotted in Fig. 2.

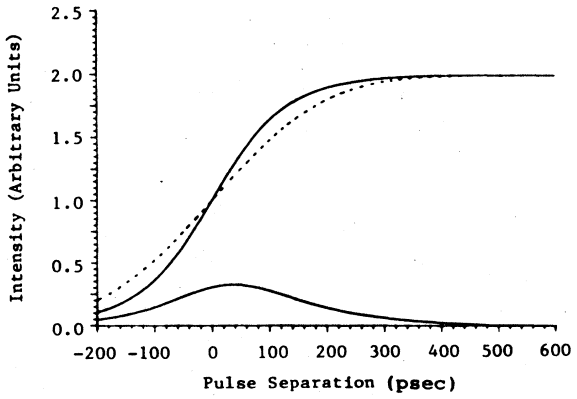

FIG. 12. Theoretical curve of Fig. 11 is replotted here along with the same theoretical calculation when the effects of noise-spike degradation are ignored; both these curves are plotted as solid lines. For comparison we also plot Yajima's formula given in Eq. (1) and normalized to the same maximum value as our result in which noise-spike degradation has been neglected; this curve is drawn as a dashed line.

average intensity of 53 kW cm^{-2} over a cross-sectional area of 0.5 cm^2. The effective area of these pulses is 3.2π while the effective noise-spike area is a factor of $\sqrt{t_c/\tau_p}$ smaller, $\theta_s=0.038\pi$. Using this value of θ_s we calculate from Eq. (25) the TDFWM signal as shown in Fig. 11. The vertical scale is arbitrary but we have used the same scale for the abscissa as in Fig. 2 to aid in comparison. The qualitative features of our data are clearly present in our calculated response. Note that we have calculated only that part of the TDFWM signal which depends on the relative decay τ; an incoherent background, independent of τ, should be added to our result.

The effect of noise-spike degradation can be appreciated if we plot the result shown in Fig. 11 together with the corresponding result when noise-spike degradation is neglected. Again we use $\theta_s=0.038\pi$ and make the comparison with the two solid traces in Fig. 12. If we use Eq. (25) in the small-pulse-area limit which leads to Eq. (1) and set $\theta_s=0.038\pi$ we obtain the dashed-line response shown in Fig. 12. This response is large inasmuch as saturation effects are not included and inherently less steep since the higher-order diagrams of Figs. 5 and 8 are not included.

A more critical test of our calculation is obtained by working with data obtained in a sample that is not optically thick. In Fig. 13(a) we plot the TDFWM signal obtained in Na vapor at 425 K when the number density is $\sim 10^{11}$ cm^{-3}. In this run we incremented the delay of the excitation pulses by approximately 5 psec between successive data points. Lack of exact synchronization with the fine-structure beating period results in the ragged appearance. If we increase the resolution we obtain the smooth response shown in Fig. 13(b). Here again the beating of the D lines is very strong. In optically thin samples we expect better agreement with our theory and indeed we find that by choosing $\theta_s=0.064$, which is within the uncertainty of what we would obtain from our measurements of pulse intensity, we obtain the solid curve which

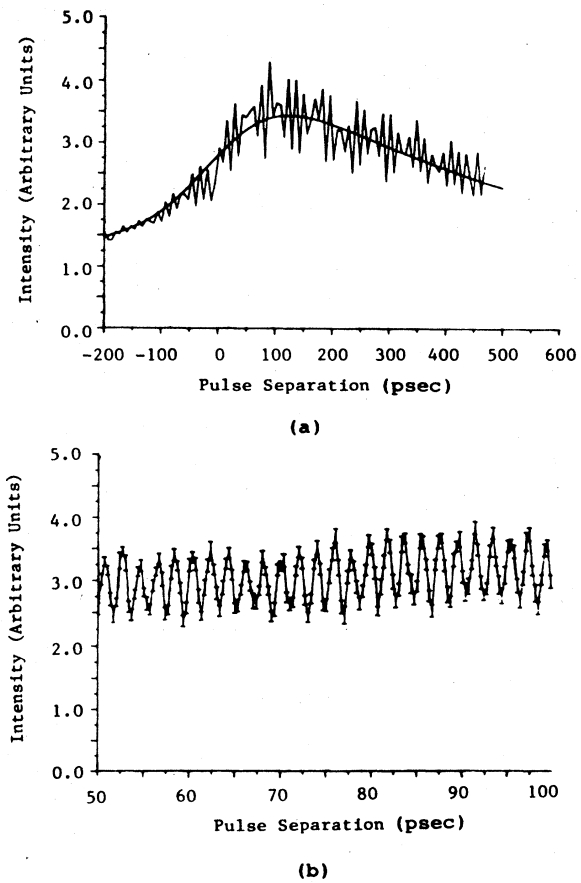

FIG. 13. (a) Experimentally measured signal intensity vs excitation pulse separation in a 10-cm-long Na cell at 425 K. In this experiment the pulse separation was stepped in approximately 5-psec increments and the excitations had a FWHM of 6 Å. Solid line represents a two-parameter fit of our theoretical expression for signal intensity given in Eq. (25). (b) Data taken under the same experimental conditions as that shown in (a) but with a finer incremental change in the excitation pulse separation. The 1.9-psec beating of the $3P$ state fine structure is clearly visible here.

passes through the data. We should note that we have also added a constant incoherent background so this curve represents a two-parameter fit.

Finally, in Fig. 14 we present data taken in a cell with temperature held fixed at 545 K, corresponding to a sodium number density of almost $\approx 10^{14}$/cm^3. There was also 1.6 torr of Ar present in the sample cell to keep the sodium from contacting and condensing on the cool end windows. The excitation pulses had a FWHM of ~ 12 Å centered at 5893 Å and intensities giving noise spikes with rms area of approximately 0.3. The remarkable feature of these data is the abrupt change in character at 0 delay. In a change of excitation delay time on the order of the field correlation time the character of the signal changes drastically in going from negative τ, where the signal is the result of accumulated free decays, to positive τ, where the

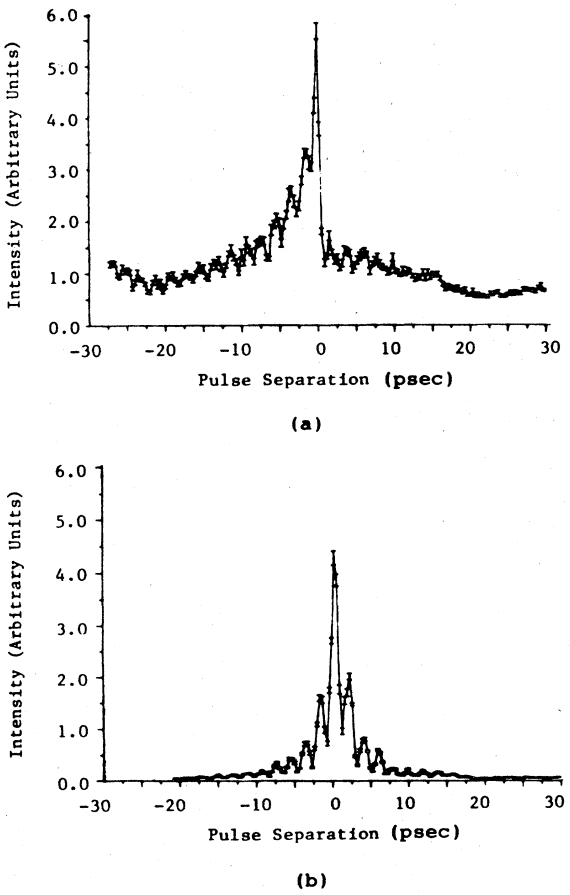

FIG. 14. (a) Data taken in a 10-cm Na cell at 545 K and an excitation pulse intensity leading to noise spikes having an rms pulse area of 0.3. In addition, 1.6 torr of argon was present in the sample cell when this data was taken. (b) Data taken under the same conditions as that shown in (a) except here the argon buffer-gas pressure is increased to 600 torr.

signal is the result of accumulated photon echoes. When the Ar buffer-gas pressure is increased to 600 torr, the signal envelope becomes symmetric around 0 delay and the background signal that was approximately independent of τ disappears. At this point we have no explanation for the anomalous behavior of the signal near $\tau=0$ taken with low perturber gas pressure.

CONCLUSION

We have presented TDFWM experimental data acquired with excitation pulse intensities at which we do not expect perturbation theory to be valid. Using a model that is similar to one already introduced to explain the photon-echo formation process[5] with excitation pulses of intense, time-separated, incoherent light, we are able to explain the general characteristics of signal versus τ curves even when pulse-induced relaxation becomes important.

Data taken at sodium number densities spanning 3 orders of magnitude is presented and the 1.9-psec fine-structure splitting of the $3P$ state of sodium is resolved. The simplicity of the technique and its applicability over such a large range of number densities suggest applications in measuring self-broadening and in plasma diagnostics.

Finally, we have presented data acquired at high sodium number density which shows anomalous behavior near $\tau=0$. Experimental and theoretical work on this problem is continuing.

ACKNOWLEDGMENTS

We would like to thank R. Kichinski for help in various stages of the experiment and B. Brody for help in preparing the manuscript. We also thank R. Friedberg for many useful discussions. This work was supported by the Joint Services Electronics Program (U.S. Army, U.S. Navy, U.S. Air Force) under Contract No. DAAG29-85-K-0049 and the U.S. Office of Naval Research.

[1]N. A. Kurnit, I. D. Abella, and S. R. Hartmann, Phys. Rev. Lett. **13**, 567 (1964).
[2]P. D. Maker and R. W. Terhune, Phys. Rev. **137**, A801 (1965).
[3]P. Ye and Y. R. Shen, Phys. Rev. A **25**, 2183 (1982).
[4]S. Asaka, H. Nakatsuka, M. Fujiwara, and M. Matsuoka, Phys. Rev. A **29**, 2286 (1984).
[5]R. Beach and S. R. Hartmann, Phys. Rev. Lett. **53**, 663 (1984).
[6]H. Nakatsuka, M. Tomita, M. Fujiwara, and S. Asaka, Opt. Commun. **52**, 150 (1984).
[7]N. Morita and T. Yajima, Phys. Rev. A **30**, 2525 (1984).
[8]The language used here is that of the "billiard-ball echo" model of Ref. 9.
[9]R. Beach, S. R. Hartmann, and R. Friedberg, Phys. Rev. A **25**, 2658 (1982).